CHINA FOUNDRY Research & Development
Vol.19 No.3 May 2022
www.springer.com/41230
https://doi.org/10.1007/s41230-022-1110-6

Effect of surface Cr/C infiltration on microstructure, mechanical properties and wear resistance of high chromium cast iron

Peng Chen[1], Zhao-yang Wu[1], **Yan-liang Yi[1, 2], Jian-bin Huang[3], Tao Shang[3], and *Wei Li[1]

1. Institute of Advance Wear & Corrosion Resistant and Functional Materials, Jinan University, Guangzhou 510632, China

2. Shaoguan Research Institute of Jinan University, Shaoguan 512027, Guangdong, China

3. Ningxia Tiandi Heavy Equipment Technology Co., Ltd., Yinchuan 753001, Ningxia, China

Abstract: A new type of high chromium cast iron (HCCI) was prepared, and its microstructure, mechanical properties, and abrasion resistance were investigated systematically. Results showed that after surface carburizing and chromizing, the microstructure of HCCI mainly consists of martensite, boride (M_2B), and carbide (M_7C_3), accompanied with a large amount of secondary precipitations $M_{23}C_6$. Moreover, the morphology and hardness of the carbide and boride in HCCI change little, while the volume fraction of carbide and boride increases from 16.23% to 23.16%. This effectively increases the surface hardness of HCCI from 64.53±0.50 HRC to 66.58±0.50 HRC, with the result that the surface of HCCI possesses a better abrasion resistance compared to the center position. Furthermore, the wear mechanism of HCCI changes from micro-plowing to micro-cutting with the increase of surface hardness.

Keywords: high chromium cast iron; carburizing and chromizing; mechanical property; abrasion resistance

CLC numbers: TG143.9 **Document code:** A **Article ID:** 1672-6421(2022)03-218-07

1 Introduction

Hammer crushers are generally used as crushing tools in the engineering field. Abrasion resistant hammers are mainly subjected to two forces in service: one is the impact force in the crushing process, and the other is the squeezing force caused by abrasive particles. This causes a severe impact which reduces the service life of hammer crushers [1-3]. Therefore, it is necessary to improve the wear performance of hammer crushers. Currently, wear-resistant metal materials include high manganese steels, low chromium cast irons, and high chromium cast irons. Compared with high manganese steels and low chromium cast irons, high chromium cast irons (HCCIs) exhibit better wear resistance in the crushing engineering field [4-8].

It is known from the Fe-C-Cr ternary phase diagram [9] that when the Cr/C ratio is high, M_7C_3 carbides form in a shape of isolated hexagonal rods or flakes. This morphology can greatly improve the continuity of the matrix, and then promote the wear resistance of HCCI. However, too high of a Cr/C ratio will consume a large amount of Cr, causing serious energy consumption. Researchers attempted to add a small amount of boride (B) into the HCCI based on a fundamental concept of replacing Cr_7C_3 with Fe_2B. Yi et al. [10] found that the microstructure mainly consisted of martensite and M_2B in the Fe-B alloys. With different B contents, the morphology and volume fraction of M_2B changed little, which contributed to the wear resistance of the material. Bedolla-Jacuinde et al. [11,12] found that the higher the B content of high chromium white cast iron, the higher the volume fraction of boron carbide. The metal matrix of high chromium white cast iron was strengthened, and the hardness was increased with the increase of B content. When the B content was 1.2wt.%, the maximum microhardness of the metal matrix of high chromium white cast iron reached 767 HV. In summary, when a small amount of B content is added to the HCCI, the morphology of carbides has little change, while the hardness of HCCI can be obviously improved as a result [13-17].

Tian et al. [18] found that the hardness of as-cast HCCI improved with the increase of Cr content. When the Cr content was 12.0wt.%, the macrohardness

***Wei Li**

Male, Professor. Research interests: wear-resistant and corrosion-resistant metal materials, metal matrix composite materials, biomedical metal functional materials and metal matrix composite materials.

E-mail: liweijn@aliyun.com

****Yan-liang Yi**

E-mail: y_yanliang@163.com

Received: 2021-05-27; Accepted: 2021-12-04

reached 61.1 HRC. Zheng et al. [19] showed that the microhardness of the matrix was increased with an increasing Cr content in the HCCI. When the Cr content was 9.7wt.%, the maximum microhardness reached 1,070.7 HV. At the same time, the wear resistance of the working surface was also significantly increased. Also, Liu et al. [20–21] found that when the C content was 3.0wt.%, the macrohardness reached 57.4 HRC; and when the C content was 3.5wt.%, the impact toughness reached 24.0 J·cm^{-2}. It can be known that the C and Cr contents have a great impact on the mechanical properties of HCCI.

In this work, a hammerhead was prepared by adding a small amount of B into the HCCI to form Fe_2B-type boride. It is known, improving the hardness and toughness of the alloy surface instead of the whole part will greatly reduce production cost. Therefore, surface carburizing and chromizing treatment was adopted to increase the amount of C and Cr in the surface of the HCCI hammerhead. The microstructure, hardness, and wear resistance of the HCCI were investigated, aiming to provide a reference to improve the service life of wear-resistant materials.

2 Materials and methods

The raw materials (ferrochromium, high chromium cast iron, carbon steel, ferromanganese, carbon powder, and pure iron) were melted and then poured at 1,580 °C into a mold. To achieve carburizing and chromizing in the hammerhead surface, a composite sand mold was used [22, 23], in which the outside layer was conventional water glass sand, while the inner layer was composed of 5% water glass, 5%–8% graphite powder, 5%–10% high chromium cast iron powder, and the balance was silica sand by weight. Heat treatment was performed for obtaining a high-strength and high-toughness matrix. The as-cast hammerhead was heated to 960 °C, held for 6 h, and then subjected to oil-cooling; followed by heating to 240 °C, holding for 3 h, and then air cooled.

The samples were wire-cut from the center (Sample 1) and surface (Sample 2) of the hammerhead and then polished to eliminate any oxidized layer. The chemical compositions were detected by an X-ray fluorescence spectrometer (SPECTROMaXx), as shown in Table 1.

Table 1: Chemical compositions of samples (wt.%)

Samples	C	Si	Mn	Cr	Mo	Cu	W	Al	Fe
1	2.681	0.721	0.435	12.421	0.140	0.126	0.014	0.058	Bal.
2	3.830	0.721	0.434	18.067	0.140	0.122	0.015	0.059	Bal.

All the metallographic samples were polished and then etched with 8vol.% nitric acid alcohol. The microstructure was observed using an optical microscope (OM, DM3000), and a scanning electron microscope (SEM, Phenom XL). Based on the OM microstructure, morphology characteristics of the carbide/boride (size, volume fraction, shape factor, etc.) were analyzed by standard inspection methods. The phase constitution was analyzed by X-ray diffractometer (Ultima lV) under a scanning speed of 5°·min^{-1} with Cu-Kα radiation at 40 kV and 200 mA in the 2θ range of 20°–90°. The corresponding composition was quantitatively analyzed by electron probe microanalysis (EPMA, JXA-8100) with the electron gun acceleration voltage of up to 30 kV, the point resolution of 1.0 nm, and the vacuum degree of 10^{-2}–10^{-4} Pa.

The microhardness was detected on a digital microhardness tester (HXD-1000TMSC/LCD) at 50 gf for 15 s, according to the GB/T 230.1-2004. The nanohardness testing of carbide and boride was performed on a nanoindentation tester (G200), according to the GB/T 25898-2010, the loading and unloading speed was 5 mN·s^{-1}, with a maximum load of 10 mN for 10 s. The macrohardness was measured by a hardness tester (HBRVU–187.5) at 1,471 N for 15 s, according to the GB/T 4340.1–1999.

Wear tests were performed on a dynamic load abrasive wear tester (MLD-10), and the related parameters are shown in Table 2. The lower sample of the friction pair was #45 steel with a macrohardness of 48–50 HRC.

Table 2: Experimental parameters of dynamic load abrasive wear tester

Parameters	Values
Impact (J)	4.5
Hammer weight (kg)	10
Impact times per minute	100
Lower sample speed (r·min^{-1})	200
Free fall height of hammer (mm)	45
Abrasive particle–quartz sand (mesh)	60–80
Abrasive flow rate (kg·h^{-1})	50
Wear time (min)	150

The worn samples were also cut from the center (Sample 1) and surface (Sample 2) of the HCCI hammerhead. The size of a sample was 10 mm×10 mm×30 mm. The worn surface was a concave surface with Φ50 mm. The test abrasive was quartz sand with a particle size of 60–80 mesh. When the wear tester was started, the abrasive flowed on the worn interface at a uniform speed of 50 kg·h^{-1}. At this time, the lower sample was rotated counterclockwise at a speed of 200 r·min^{-1} for 30 min, while the upper sample was moved up and down. After each test, the samples were ultrasonically cleaned with alcohol, dried with a hairdryer, and weighed by an analytical balance with an accuracy of 0.0001 g. Each test was repeated for six groups. The worn surface was examined by SEM (Phenom XL) and color

3D-laser scanning microscopy (MFT-5000) to analyze wear characteristics.

3 Results and discussion

3.1 Microstructures

Figures 1 and 2 show the XRD patterns and OM morphologies of the samples, respectively. From Fig. 1, it can be known that the matrix of all the samples mainly consists of α-Fe (JCPDS 06-0696), M_7C_3, and $M_{23}C_6$ (M represents Cr, Mn, and Fe). As shown in Fig. 2, the α-Fe is tempered martensite, and lots of secondary precipitations $M_{23}C_6$ separate from the martensite. Moreover, lots of rod-, net-, and block-shaped M_7C_3 hard phase and a little network M_2B boride are observed. The amount of M_2B is too small to be detected in the XRD pattern.

A Fe-C-Cr ternary phase diagram [24] shows that there are three types of carbides in the HCCI: M_3C-type, M_7C_3-type, and $M_{23}C_6$-type. M_3C-type carbides are prone to appear in high-carbon and low-chromium conditions, $M_{23}C_6$-type carbides are easily formed in low-carbon and high-chromium conditions, while M_7C_3-type carbide is only obtained when the ratio of Cr/C is appropriate, generally no less than 5. The hardness of M_7C_3-type carbide is relatively high, and it is distributed in the shape of isolated hexagonal rods or flakes. As a result, the degree of carbide splitting on the matrix is greatly reduced, and then the continuity of the matrix is greatly improved.

Figure 3 shows EPMA mapping distribution of elements in Sample 2. It shows that Cr is mainly dissolved in the carbides, and partially dissolved in the matrix, which improves the hardenability of HCCI. Moreover, C and B are mainly dissolved in the carbide or boride. Related reports [25, 26] showed that almost all the B atoms existed in the form of the B-C compounds. Table 3 shows EPMA mapping scanning results of Samples 1 and 2. It can be seen that the B contents of Samples 1 and 2 are 0.35wt.% and 0.38wt.%, respectively. Moreover, it can also be seen that the C and Cr contents of the Sample 1 are 2.77wt.% and 13.12wt.%, respectively, while those of Sample 2 are 3.69wt.% and 18.62wt.%, respectively. This shows that the carburizing and chromizing treatment can effectively improve the C and Cr contents of the hammerhead surface.

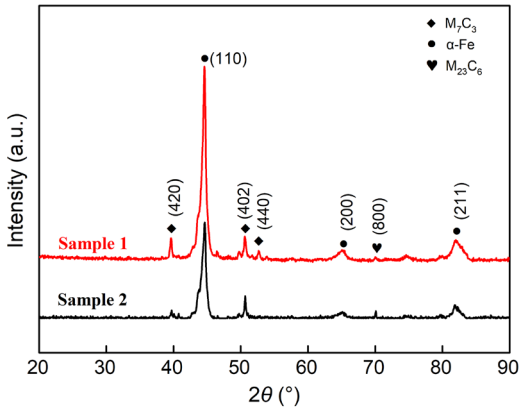

Fig. 1: XRD patterns of Samples 1 and 2

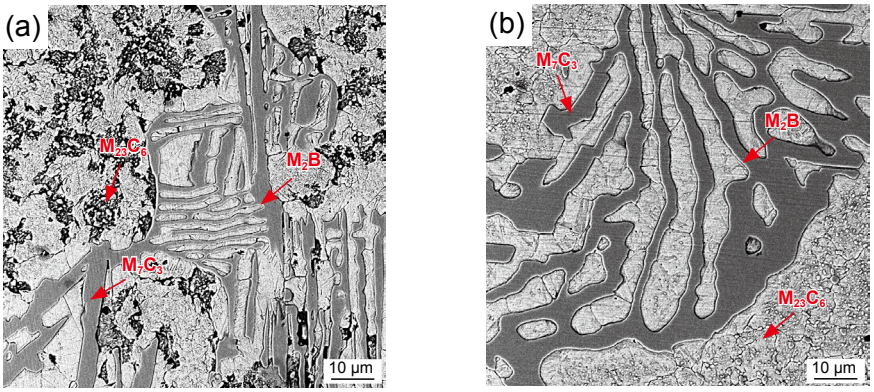

Fig. 2: SEM morphologies of high chromium cast iron: (a) Sample 1; (b) Sample 2

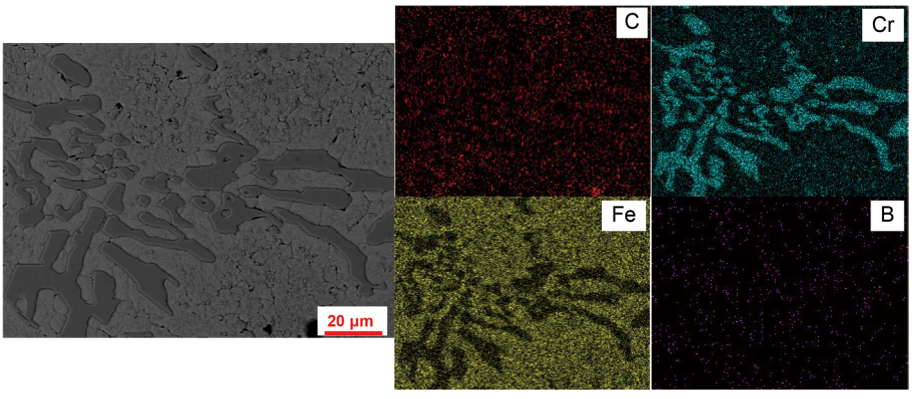

Fig. 3: Mapping distribution of alloying elements of Sample 2

Table 3: EPMA mapping scanning results of Samples 1 and 2

Samples	B	C	Cr	Fe
1	0.35	2.77	13.12	80.72
2	0.38	3.69	18.62	75.29

To quantitatively evaluate the morphology of hard phase (M_7C_3 and M_2B), the corresponding characterization is performed by randomly selecting OM figures, measuring the area (A) and circumference (L) of hard phase using DT2000 software. On this basis, the shape factor (K) and particle size factor (D) of the hard phase can be calculated as follows [27]:

$$\begin{cases} K = \dfrac{4\pi A}{L^2} \\ D = 2\sqrt{\dfrac{A}{\pi}} \end{cases} \quad (1)$$

where, the K value ranges from 0 to 1. The closer the K value is to 1, the more spherical the carbide and boride. The smaller the D value, the finer the carbide and boride particles. According to Eq. (1), the K and D values of Sample 1 are 0.13 and 11.95 μm, while those of Sample 2 are 0.14 and 11.91 μm, respectively. This shows that the carburizing and chromizing treatment has little influence on the morphology and size of the carbide and boride in the HCCI.

According to the National Standard GB/T 6394-2002 [28], the grain sizes of the metal matrix in the Samples 1 and 2 were measured. Representative fields were selected to measure the average grain size, as shown in the different color areas of Fig. 4. The grain sizes of the metal matrix in Samples 1 and 2 are 9.0 μm and 8.0 μm, respectively. It can be known that the grain size of the metal matrix has little change after surface carburizing and chromizing. In other words, there is no grain refinement strengthening contribution to the metal matrix in the HCCI after carburizing and chromizing.

To count the volume fraction of hard phase in the HCCI, the metallographic microstructure was colorized and calibrated by using PhotoShop software, as shown in Fig. 5. The red region in Fig. 5(b) shows the hard phase. The DT2000 software was used to automatically count the proportion of the red region, obtaining the volume fraction, as shown in Fig. 6. It can be seen that the volume fraction of hard phases decreases gradually from surface to the center. The volume fraction of hard phase in the center is 16.23vol.%, while that in the surface is 23.16vol.%. This is mainly caused by the gradual increase of C and Cr content from center to surface after carburizing and chromizing.

3.2 Mechanical properties

Figure 7 shows the P-h curves of Cr_7C_3 and M_2B obtained from the nanoindentation test. The test results are shown in Table 4. It is found that the hardness of the network boride (M_2B) is

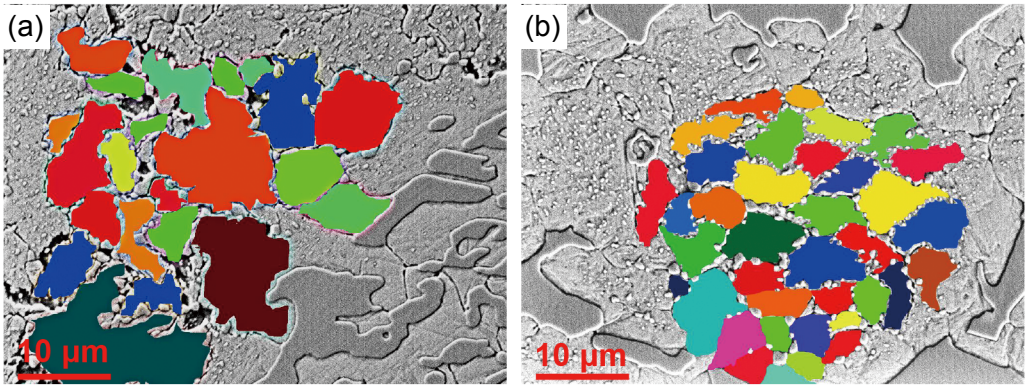

Fig. 4: Grain size statistics of high chromium cast iron at different positions: (a) Sample 1; (b) Sample 2

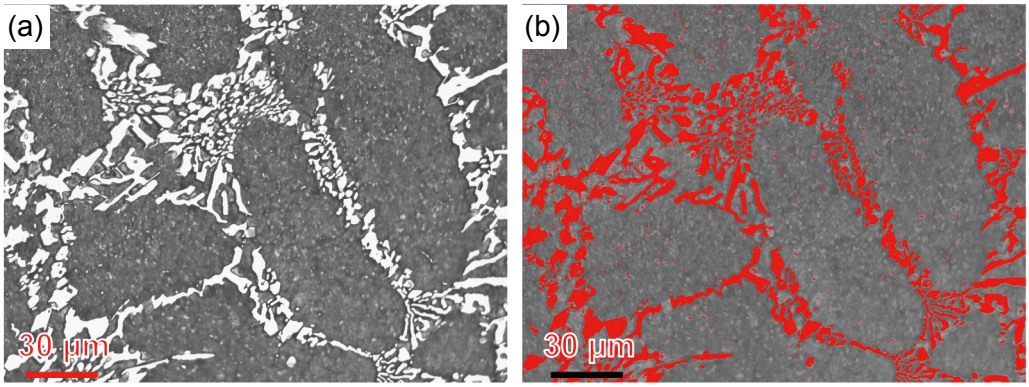

Fig. 5: Typical microstructure of hard phase in the high chromium cast iron: (a) original microstructure; (b) calibrated microstructure

23.52±1.08 GPa, while the hardness of the rod-shaped carbide (M_7C_3) is 19.32±1.26 GPa. Visibly, the M_2B has a higher hardness compared to the M_7C_3, thus it can make a positive contribution to the hardness of the HCCI. The elastic modulus can be regarded as an index to access the elastic deformation of the material. The higher the elastic modulus, the greater the stress causing a certain elastic deformation. It can also be said that under certain stress, the smaller the elastic deformation. Compared to the M_7C_3, the M_2B has a higher elastic modulus, showing that it possesses a better fracture toughness.

Table 5 shows the microhardness results of various phases from surface to center in the HCCI. For the matrix, the microhardness increases gradually from center to surface. The microhardness at the center is about 753.8 HV, while that at the surface is about 860.5 HV. This is because the contents of C and Cr in the matrix increase gradually from center to surface in the HCCI, and more C and Cr content dissolve into the matrix at the surface, resulting in a greater strengthening effect. However, the change of C and Cr content has little influence on the hardness of the hard phase in the HCCI: the microhardness of M_7C_3 is about 1,500 HV, and that of M_2B is about 1,600 HV.

A rectangular parallelepiped sample of 150 mm×55 mm×25 mm was cut from the riser to measure the macrohardness along the radial direction of A-A and the vertical direction of B-B, as shown in Fig. 8, with an interval of 2.0 mm. The results are shown in Fig. 9. It can be seen that the depth of carburizing and chromizing layer is 8.0–10.0 mm. The surface layer is 66.58±0.50 HRC, while that in the center position is 64.53±0.50 HRC. This mainly contributed to the increased volume fraction of hard phase because of the carburizing and chromizing treatment.

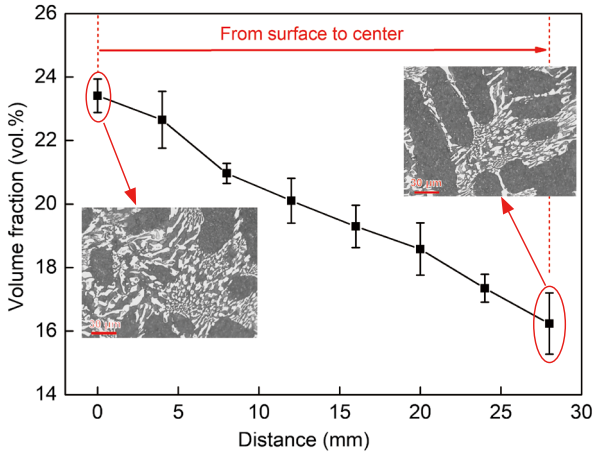

Fig. 6: Volume fraction distribution of hard phase in the high chromium cast iron

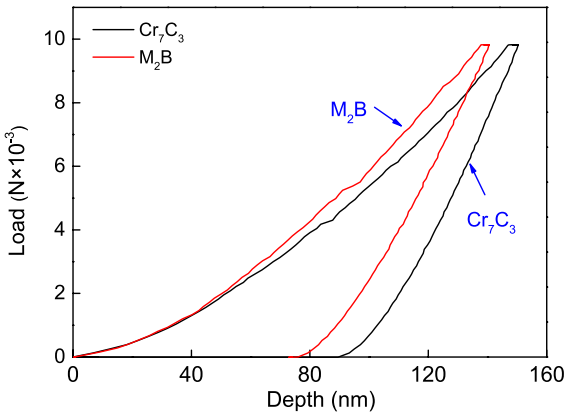

Fig. 7: *P-h* curves of Cr_7C_3 and M_2B obtained from nanoindentation test

Table 4: Nanoindentation test results

Phase	Elastic modulus (GPa)	Nanohardness (GPa)
M_2B	352.07±3.48	23.52±1.08
M_7C_3	343.34±4.05	19.32±1.26

Table 5: Microhardness of the high chromium cast iron from surface to center

Distance (mm)	Matrix (HV)	M_7C_3 (HV)	M_2B (HV)
0	860.5	1,538.1	1,628.2
5.0	846.1	1,531.6	1,625.0
10.0	830.0	1,528.4	1,618.6
15.0	815.3	1,511.6	1,610.4
20.0	792.6	1,508.1	1,600.0
25.0	773.1	1,500.4	1,595.0
30.0	753.8	1,496.8	1,573.8

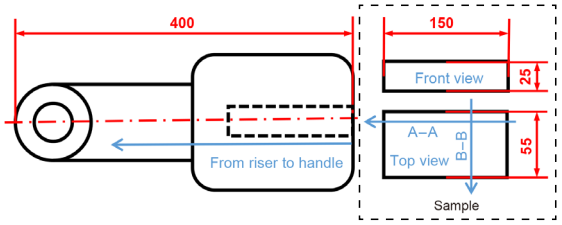

Fig. 8: Schematic diagram of the hammerhead and marking of its measuring track

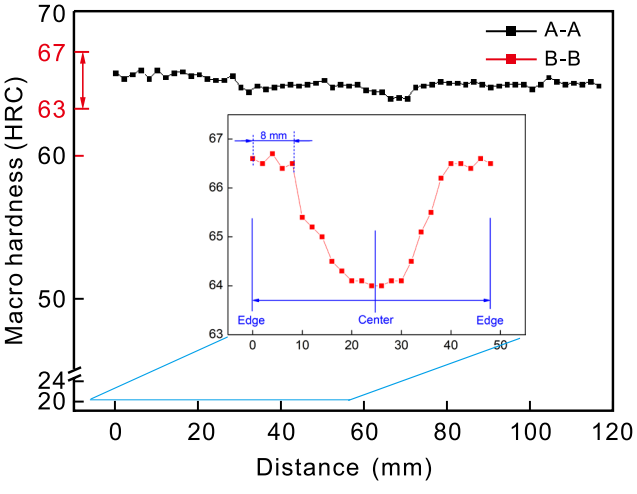

Fig. 9: Macrohardness distribution of different positions in the high chromium cast iron hammerhead

3.3 Dynamic load abrasive wear test

The wear test data shows that the wear weight loss of Sample 1 is 0.5444 g, while that of Sample 2 is 0.4807 g. This indicates that Sample 2 possesses a better abrasion resistance.

Figures 10(a) and (b) show the SEM morphologies of worn surfaces in Samples 1 and 2. For Sample 1, deep and wide furrows cover the entire worn surface, and obvious wedge deformation occurs at the two sides of furrows, followed by severe fragmentation and delamination. The wear mechanism is dominated by a mixed mode of micro-plough and micro-cutting. For Sample 2, the ploughing grooves are shallower and narrower compared to Sample 1, and slighter delamination and fragmentation occur in the worn surface. This indicates that the wear mechanism of Sample 2 changes into micro-cutting accompanied by slightly micro-plough. Figures 10(c) and (d) show the 3D morphology of the worn surface of Samples 1 and 2, respectively. After abrasive wear, some furrows and spalling pits are formed on the worn surface, which is very consistent with the SEM morphologies.

The profile of the worn surfaces is measured by a 3D-laser scanning microscope in a length of about 200 μm, and the corresponding surface roughness of Samples 1 and 2 is listed in Table 6. The average roughness (R_a) is defined as the length from the peak to the valley along the center line. Root mean square roughness (R_q) is defined as the root mean square value of the contour offset within the sampling length. The maximum height of the roughness (R_t) is defined as the maximum peak-to-valley height within the profile evaluation length. The average maximum height of the profile (R_z) is defined as the height of the sum of the maximum profile peak height and the maximum profile valley depth within a sampling length.

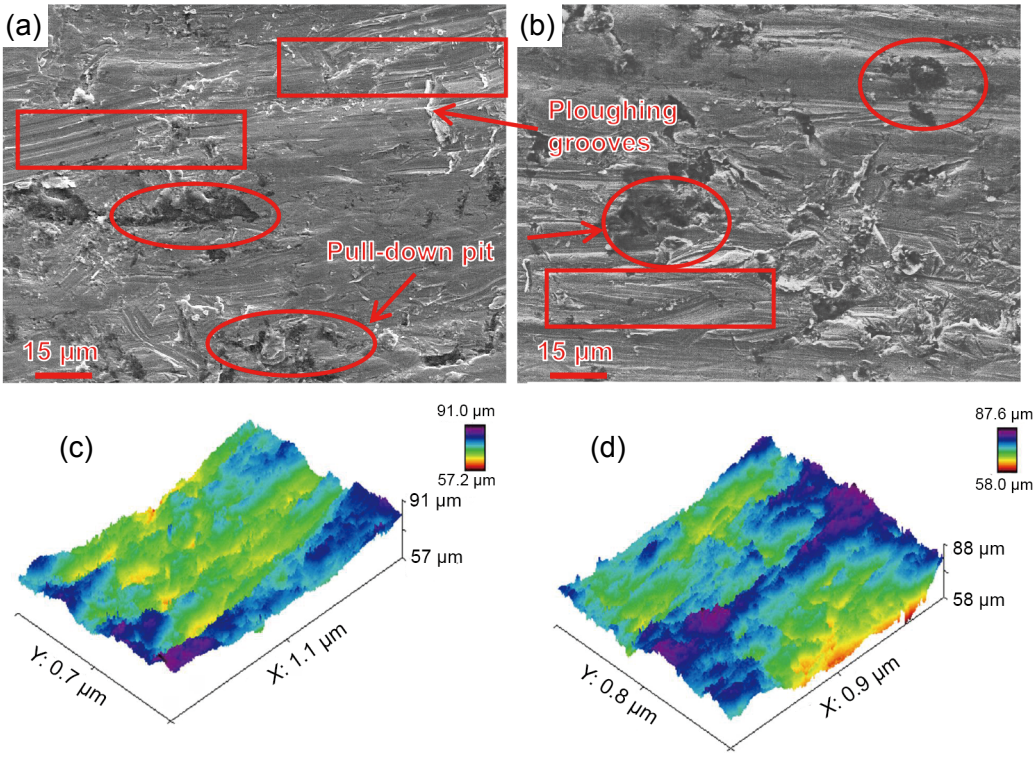

Fig. 10: SEM and 3D morphologies of worn surface in HCCI: (a, c) Sample 1; (c, d) Sample 2

Table 6: Measurements of surface roughness of Samples 1 and 2 (μm)

Samples	R_a	R_q	R_t	R_z
1	0.320	0.472	3.835	3.714
2	0.287	0.396	3.535	2.891

4 Conclusions

The microstructure, mechanical properties, and wear resistance of a new type of high chromium cast iron were systematically investigated. The results obtained are summarized as follows:

(1) After heat treatment, the microstructure of high chromium white cast iron mainly contains carbide (M_7C_3), tempered martensite, secondary precipitated phase $M_{23}C_6$, and a small amount of M_2B.

(2) After surface carburizing and chromizing, the morphology and hardness of the hard phase (M_2B and M_7C_3) have little change, while its volume fraction changes from 16.23vol.% (center) to 23.16vol.% (surface), and the macrohardness of HCCI changes from 64.53±0.50 HRC to 66.58±0.50 HRC from center to surface.

(3) In the process of impact abrasive wear, the wear mechanism changes from micro-ploughing to micro-cutting after surface carburizing and chromizing. The surface possesses a higher abrasion resistance compared to the center position in the HCCI, due to more hard phase forming in the surface.

Acknowledgements

This study was financially supported by the National Key Research and Development Project of China (No. 2017YFB0305100), the Science and Technology Project of Guangdong Province (No. 2017B090903005), the National Natural Science Foundation of China (No. 52005217), the Science and Technology Project of Guangzhou City (No. 201806040006), the Basic and Applied Basic Research Fund Project of Guangdong Province (Nos. 2021A1515010523 and 2020A1515110020), and the Fundamental Scientific Research Business Expenses of Central Universities (No. 21620344).

References

[1] Mao J B. Development of new wear-resistant materials for crusher hammers and their manufacturing process. Cement, 1997(7): 22–25. (In Chinese)
[2] Ibrahim M M, El-Hadad S, Mourad M. Influence of niobium content on the mechanical properties and abrasion wear resistance of heat-treated high-chromium cast iron. International Journal of Metalcasting, 2021, 15(2): 500–509.
[3] Guo K X, Xia P J. Research progress and prospects of wear resistance of high chromium cast iron. Foundry Technology, 2018, 39(9): 2138–2141. (In Chinese)
[4] Zhang F Q, Li L M, Chen Y X, et al. Development and application of large low-alloy steel wear-resistant hammerhead. Foundry, 2011, 60(2): 195–198. (In Chinese)
[5] Shah M, Sahoo K L, Das S K, et al. Wear mechanism of high chromium white cast iron and its microstructural evolutions during the comminution process. Tribology Letters, 2020, 68(3): 77, doi: 10.1007/s11249-020-01317-6.
[6] Li M L, Mao J B. Development and selection of new wear-resistant material use for hammering shatter machine ram. Water Conservancy and Electric Power Machinery, 1999(5): 43–46.
[7] Li F Y, Liu Y. Heat treatment of high chromium white cast iron. Journal of Liaoning Technical University, 2005(S2): 236–238. (In Chinese)
[8] Wan J, Lu Y R, Qing J J, et al. Developing a M_6C-reinforced high-Cr white iron for abrasive wear application. Metallurgical and Materials Transactions A, 2021, 52: 1976–1984.
[9] Jackson R S. The austenite liquidus surface and constitutional diagram for the Fe-Cr-C metastable system. Journal of the Iron and Steel Institute, 1970, 208(2): 163. (In Chinese)
[10] Yi Y, Xing J, Lu Y, et al. Investigations on microstructure, mechanical properties and abrasion resistance of 4wt.% Cr -2wt.% Mn-2wt.% Cu-Fe-B alloy. Materials Characterization, 2018, 137: 222–230.
[11] Huang Z F, Xing J D, Gao Y M. Effect of boron on the microstructure and properties of semisolid hypereutectic high chromium cast iron. Rare Metal Materials and Engineering, 2011, 40(S2): 244–247.
[12] Bedolla-Jacuinde A, Guerra F V, Guerrero-Pastran A J, et al. Microstructural effect and wear performance of high chromium white cast iron modified with high boron contents. Wear, 2021, 476: 203675, doi: 10.1016/j.wear.2021.203675.
[13] Chung R J, Tang X H, Li D Y, et al. Microstructure refinement of hypereutectic high Cr cast irons using hard carbide-forming elements for improved wear resistance. Wear, 2013, 301(1–2): 695–706.
[14] Zheng S. Research on the microstructure and mechanical properties of austempered high boron white cast iron. Master Thesis, Beijing: Tsinghua University, 2012. (In Chinese)
[15] Wang K K, Wang R F, Wu R R, et al. Effect of boron the microstructure and properties of Cr27 high chromium cast iron. Casting Technology, 2017, 38(10): 2344–2347, 2364. (In Chinese)
[16] Ma S Q, Xing J D, Fu H G, et al. Interface characteristics and corrosion behavior of oriented bulk Fe_2B alloy in liquid zinc. Science, 2014(78): 71–80.
[17] Ma S Q, Xing J D, He Y L, et al. Effect of orientation and lamellar spacing of Fe_2B on interfaces and corrosion behavior of Fe-B alloy in hot-dip galvanization. Acta Materialia, 2016,115: 392–402.
[18] Tian Y, Ju J, Fu H G, et al. Effect of Chromium content on microstructure, hardness, and wear resistance of as-cast Fe-Cr-B alloy. Journal of Materials Engineering and Performance, 2019, 28(10): 6428–6437.
[19] Zheng B C, Huang Z F, Xing J D, et al. Two-body abrasion resistance of cementite containing different chromium concentrations. Journal of Materials Research, 2016(31): 655–662.
[20] Liu Y, Xia Q. Influence of carbon content on the microstructure, hardness and impact toughness of high chromium white cast iron. Journal of Luoyang Institute of Technology, 1999(4): 21–24. (In Chinese)
[21] Zhu G Q, Zheng Z F, Zhang M X. Effect of chromium on properties of low carbon high chromium cast iron. Hot Working Technology, 2008(1): 15–17. (In Chinese)
[22] Chen W C. Experimental research on a new type of inlaid wear-resistant hammer. Sichuan Cement, 2019(8): 143. (In Chinese)
[23] Li M, Cheng J Q, Gao Z C, et al. Development of wear-resistant materials for crusher hammers and their manufacturing process. Mining Machinery, 2012, 40(7): 67–71.(In Chinese)
[24] Tabrett C P, Sare I R, Ghomashchi M R. Microstructure-property relationships in high chromium white iron alloys. International Materials Reviews, 1996, 41(2): 59–82.
[25] Jian Y X, Huang Z F, Xing J D, et al. Effect of improving Fe2B toughness by chromium addition on the two-body abrasive wear behavior of Fe-3.0wt.% B cast alloy. Tribology International, 2016, 101: 331–339.
[26] Jian Y X, Huang Z F, Xing J D, et al. Effects of Mn addition on the two-body abrasive wear behavior of Fe-3.0wt.% B alloy. Tribology International, 2016, 103: 243–251.
[27] Hong G. Ore properties of Henan bauxite and their influence on ore dressing and metallurgy. Mining and Metallurgy, 2002(1): 27–32. (In Chinese)
[28] Wang K Y. Introduction to GB/T 6394-2002: Metal average grain size measurement method. Standardization and Quality of Machinery Industry, 2004(5): 5–8. (In Chinese)
[29] Zhou Q D, Su J. Chromium family of wear resistant cast iron. Xi'an, China: Xi'an Jiaotong University Press, 1986: 111–112. (In Chinese)